

# Direct transition between quantum spin Hall and ordinary insulating phases induced by spin-mixing tunneling in symplectic disordered quantum spin Hall systems

Jie Lu\*

*College of Physics, Hebei Advanced Thin Films Laboratory,  
Hebei Normal University, Shijiazhuang 050024, China*

Mei Li

*School of Physics and Technology, Center for Electron Microscopy and MOE Key Laboratory  
of Artificial Micro- and Nano-structures, Wuhan University, Wuhan 430072, China*

(Dated: March 23, 2017)

The disordered quantum spin Hall (QSH) systems with spin-mixing tunneling (SMT) at potential saddle points, which belong to the Wigner-Dyson symplectic class AII, are revisited in detail using an existing spin-directed quantum network model generalized from the Chalker-Coddington random network model. A new phase diagram is obtained in which the ordinary insulating (OI) phase fills the whole parameter space and the QSH state only survives on a line segment of the boundary where SMT is absent. Thus a direct transition from QSH to OI phases exists and is driven by the SMT since it induces backscattering between the Kramers doublets at the same edge and thus completely destroys them. To verify these results, finite-size analyses of the two-terminal conductance and normalized localization length of electrons are performed following standard numerical algorithms. Numerics clearly shows that once the SMT is switched on, neither marginal dissipationless channels nor bulk metallic states survive when the system size is large enough.

PACS numbers: 71.70.Ej, 72.15.Rn, 73.20.Fz, 73.43.Nq

## I. INTRODUCTION

Anderson transition, i.e., transitions between localized and delocalized quantum phases in disordered electronic systems, has attracted intense and continuous attention since its proposal[1] due to its fundamental significance in condensed matter physics[2–5]. In 1970s and 1980s, scaling-theory and field-theory approaches revealed the connections between Anderson transition and conventional second-order phase transitions[2–4]. In 1990s, the symmetry classification of disordered systems was achieved based on its relation to the classical symmetric spaces[6–8]. Later, the completeness of this classification is proved in 2005[9]. Now we know there are totally ten symmetry classes according to how many discrete symmetries are obeyed by the underlying physical system. When a system only has symmetries translationally invariant in energy, such as the time-reversal symmetry (TRS) and spin-rotation symmetry (SRS), it falls into one of the three traditional Wigner-Dyson classes (unitary, orthogonal and symplectic)[10, 11]. However, if we focus on some particular value of energy, extra discrete symmetries could arise and lead to novel symmetry classes. In condensed matter systems described by a tight-binding model on a bipartite lattice with randomness only residing in hopping terms, three chiral classes are identified[6]. The remaining four classes were discovered in superconducting systems and now known as the Bogoliubov-de Gennes classes[7]. In the past decades, Anderson transitions in these ten classes have been investigated intensively and considerable progress has been made in various directions, such as their scaling-

theory and field-theory descriptions[2–4], multifractality in critical wave functions[12–18] and level statistics at criticality[19–23], etc.

Recently, the spin-orbit-induced topological materials, named as topological insulators (TIs), have received intensive attention[24–30]. In TIs, the interplay between topology and symmetry greatly enriches our knowledges of quantum states[30–33]. First, the TRS is crucial for their realization and stabilization. Second, the spin-orbit coupling (SOC) destroys the SRS, thus makes TI belong to the symplectic Wigner-Dyson class AII. In two dimensions (2D), they are the well-known quantum spin Hall (QSH) ensembles. In disordered QSH systems, the term “Anderson transition” can be extended from traditional metal-insulator transitions to a broader sense which also includes transitions between topologically trivial and nontrivial phases[5]. *Thus, it is natural to ask whether a direct transition between ordinary insulating (OI) and QSH phases exists or not in symplectic disordered QSH systems independent of microscopic models.* In the past decade, great efforts have been devoted into this problem[33–41]. Based on some network model of QSH systems, several numerical works declare that for symplectic class AII, the OI and QSH phases are separated by intermediate metallic phase everywhere in the phase space[33–38]. In this work, we revisit this quantum network model in which a spin-mixing tunneling (SMT) at the saddle points (SPs) of random electronic potential is introduced meanwhile the scattering matrix still preserves TRS. A new phase diagram is obtained indicating that a direct transition between QSH and OI phases exists and driven by the SMT since it induces backscat-

tering between the Kramers pairs at the same edge and thus completely destroys them.

This paper is organized as follows. In Sec. II the spin-directed quantum network model with SMT for disordered QSH systems is reviewed. In particular, the algorithms for calculating the two-terminal conductance and the normalized localization length are presented in detail for verification. Based on this model, in Sec. III we numerically study the quantum phases in symplectic disordered QSH systems and obtain a new phase diagram. In the last section, the concluding remarks are provided.

## II. MODELING AND METHODOLOGY

### II.A Brief review of Chalker-Coddington random network model

Under a strong magnetic field  $\vec{B} = B\hat{z}$ , the motion of an electron in a 2D smooth potential  $V(\vec{r})$  can be decomposed into a rapid cyclotron gyration and a slow drift of the guiding center along an equipotential contour which is generally composed of numerous loops around potential valleys or peaks[42, 43]. The drifting direction of electrons in each loop is uni-directional (chiral):  $\vec{v}(\vec{r}) = \nabla V(\vec{r}) \times \vec{B}/(eB^2)$ . Electrons flow along equipotential lines and their mutual tunneling at potential SPs are the essential physical ingredients for constructing a network model describing quantum criticality in disordered 2D systems. For modelization, the potential SPs are arranged to form a 2D square lattice with the interconnected links representing the electron flows along equipotential lines. The potential peaks and valleys distribute alternatively in the square plaquettes enclosed by the links. This endues definite propagating direction of electron flows on the links and then divides the SPs into two subgroups: the S- and S'-types, as shown in Fig. 1a and 1b. At each SP, two incoming and two outgoing electron flows intersect hence lead to a  $2 \times 2$  scattering matrix. Disorder can be introduced by random phases along links and/or the heights of SPs. At last, quantum tunneling only occurs at SPs and in the simplest case can be assumed uniform. This is the basic framework of the Chalker-Coddington random network model (CC-RNM).

### II.B Spin-directed quantum network model

To study Anderson transitions in disordered QSH systems, the CC-RNM should be generalized to include the spin degree of freedom. This leads to the spin-directed quantum network model (SD-QNM) proposed in Refs.[33–37]. As shown in Fig. 1c and 1d, the original uni-directed electron flow on each link is generalized to a Kramers doublet, that is, a pair of current paths in

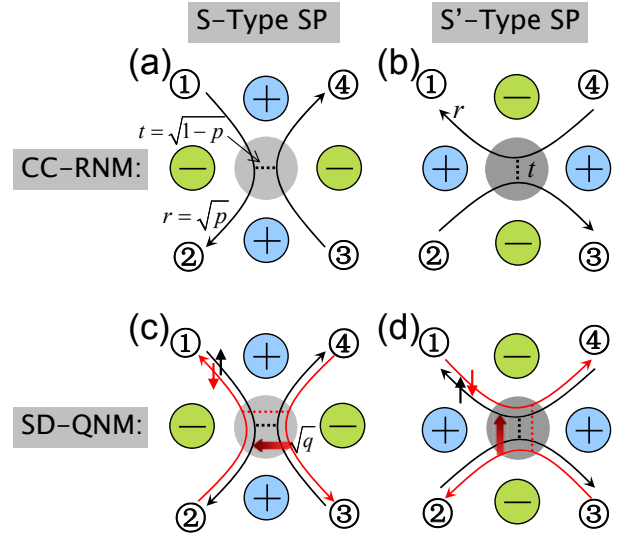


FIG. 1: (Color online) Schematics of CC-RNM and SD-QNM. (a) and (b) show the S- and S'-type SPs in CC-RNM. At each SP, two incoming and two outgoing electron flows intersect with tunneling amplitude  $\sqrt{1-p}$ . Blue (green) circles with “+(-)” inside denote the potential peaks (valleys). (c) and (d) show the counterparts of (a) and (b) in SD-QNM where the spin degree of freedom is included. The original chiral electron flow on each link is generalized to a Kramers doublet. Throughout this paper, black (red) means spin-up (-down). In addition, at each SP a SMT with amplitude  $\sqrt{q}$  is introduced and depicted by the reddish black arrow.

which electrons with opposite spins propagate in opposite directions. Therefore, the scattering matrix of each SP becomes  $4 \times 4$ . For simplicity, disorder is introduced only through random phases on each link. For S-type SP, the scattering matrix at position  $\mathbf{R}$  reads,

$$\begin{pmatrix} Z_{2\uparrow}^{\text{out}} \\ Z_{1\downarrow}^{\text{out}} \\ Z_{4\uparrow}^{\text{out}} \\ Z_{3\downarrow}^{\text{out}} \end{pmatrix} = s_{\mathbf{R}} \begin{pmatrix} Z_{1\uparrow}^{\text{in}} \\ Z_{2\downarrow}^{\text{in}} \\ Z_{3\uparrow}^{\text{in}} \\ Z_{4\downarrow}^{\text{in}} \end{pmatrix}, \quad s_{\mathbf{R}} = \Theta_{\mathbf{R}}^{2143} S \Theta_{\mathbf{R}}^{1234}. \quad (1)$$

where  $Z_{j\sigma}^{\text{out(in)}}$  is the electron flow amplitude at link  $j$  with spin  $\sigma$  ( $\uparrow$  or  $\downarrow$ ),  $\Theta_{\mathbf{R}}^{jklm}$  is a diagonal matrix,

$$\Theta_{\mathbf{R}}^{jklm} \equiv \text{diag} \left( e^{i\theta_{\mathbf{R}}^j}, e^{i\theta_{\mathbf{R}}^k}, e^{i\theta_{\mathbf{R}}^l}, e^{i\theta_{\mathbf{R}}^m} \right). \quad (2)$$

Here  $e^{i\theta_{\mathbf{R}}^j}$  is the phase an electron acquires when propagating on link  $j$  between the observation point and the SP at node- $\mathbf{R}$ . We have neglected the spin index since the Kramers pair of electron flows have the same accumulated phase on the same link. To mimic the randomness in SP distribution, these phases are distributed uniformly and independently in the region  $[0, 2\pi)$ . The matrix  $S$  describes the percolation and tunneling at a S-type SP and has the following structure[33–37],

$$S = \begin{pmatrix} \sqrt{p} I_{2 \times 2} & \sqrt{1-p} Q \\ \sqrt{1-p} Q^\dagger & -\sqrt{p} I_{2 \times 2} \end{pmatrix}, \quad (3)$$

where  $I_{2 \times 2}$  is the unit matrix and

$$Q = \begin{pmatrix} \sqrt{1-q} & \sqrt{q} \\ -\sqrt{q} & \sqrt{1-q} \end{pmatrix}. \quad (4)$$

The parameter  $p$  is related to the chemical potential of the system, with  $\sqrt{1-p}$  measuring the quantum tunneling amplitude at a SP for both up and down spins due to the TRS. While  $\sqrt{q}$  describes the SMT strength of electron flows at the SPs. Rotating Eq. (1) by 90 degrees, the scattering matrix  $S'$  of the S'-type SP at node- $\mathbf{R}'$  is then obtained. The above choice of scattering matrices at SPs and random phases along links preserves TRS, i.e.

$$X^\dagger = \begin{pmatrix} \sigma_y & 0 \\ 0 & \sigma_y \end{pmatrix} X^* \begin{pmatrix} \sigma_y & 0 \\ 0 & \sigma_y \end{pmatrix}, \quad X = S \text{ or } S', \quad (5)$$

but breaks SRS, thus realizes a quantum network model of Wigner-Dyson symplectic class AII.

It is worth emphasizing that the SMT at potential SPs is different from the SOC responsible for the formation of QSH states. First, the SOC exists across all of the real lattice nodes while the SMT is present only at potential SPs. More important, the SOC comes from the lack of macroscopic or microscopic inversion symmetry. It replaces the role of periodic magnetic flux and manifests itself as additional terms in the system Hamiltonian to couple spin-up and spin-down components. The real spin is then no longer a good quantum number. In many cases, the quantum number of new eigenstates which are superpositions of original up and down spins is still called “spin”, however one must bear in mind that it actually denotes the new good quantum number of the Kramers doublet. The SMT then occurs between electron flows with different new “spin” and have off-diagonal elements rather than the SOC.

### II.C Two-terminal conductance

Now we consider a 2D SP lattice composed by  $L$  principal layers (PLs), as shown in Fig. 2. Each PL consists of  $W$  S-type and  $W$  S'-type SPs. In SD-QNM, there are totally  $8WL$  electron flows on this lattice. At a S-type SP at node- $\mathbf{R}$ , the left-to-right transfer matrix is obtained from its scattering matrix as

$$\begin{pmatrix} Z_{4\uparrow}^{\text{out}} \\ Z_{4\downarrow}^{\text{in}} \\ Z_{3\uparrow}^{\text{in}} \\ Z_{3\downarrow}^{\text{out}} \end{pmatrix} = T_{\mathbf{R}} \begin{pmatrix} Z_{1\uparrow}^{\text{in}} \\ Z_{1\downarrow}^{\text{out}} \\ Z_{2\uparrow}^{\text{out}} \\ Z_{2\downarrow}^{\text{in}} \end{pmatrix}, \quad T_{\mathbf{R}} = C (P_{\mathbf{R}} \otimes Q_{\mathbf{R}}^\dagger) C, \quad (6)$$

in which

$$P_{\mathbf{R}} = \begin{pmatrix} \frac{1}{\sqrt{1-p}} e^{i\eta_{11}} & -\sqrt{\frac{p}{1-p}} e^{i\eta_{12}} \\ -\sqrt{\frac{p}{1-p}} e^{i\eta_{21}} & \frac{1}{\sqrt{1-p}} e^{i\eta_{22}} \end{pmatrix}, \quad (7)$$

$$\eta_{11} = (\theta_{\mathbf{R}}^1 + \theta_{\mathbf{R}}^2 + \theta_{\mathbf{R}}^3 + \theta_{\mathbf{R}}^4) / 2 = -\eta_{22},$$

$$\eta_{12} = (\theta_{\mathbf{R}}^3 + \theta_{\mathbf{R}}^4 - \theta_{\mathbf{R}}^1 - \theta_{\mathbf{R}}^2) / 2 = -\eta_{21},$$

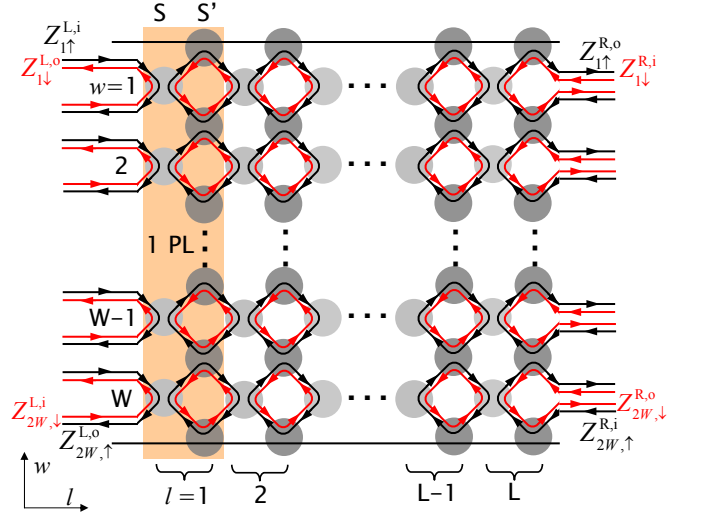


FIG. 2: (Color online) Schematic of the layout of a SD-QNM network with RBC for calculating the two-terminal conductance. The light (dark) gray circles indicate S-type (S'-type) SPs. The 2D SP lattice is composed of  $L$  PLs. Each PL (orange vertical stripe) consists of  $W$  S-type and  $W$  S'-type SPs. On each side of the system,  $2W$  incoming and  $2W$  outgoing electron flows distribute alternatively and related by the total transfer matrix  $T_W^L$ .

$$Q_{\mathbf{R}} = \begin{pmatrix} \sqrt{1-q} e^{i\zeta_{11}} & \sqrt{q} e^{i\zeta_{12}} \\ -\sqrt{q} e^{i\zeta_{21}} & \sqrt{1-q} e^{i\zeta_{22}} \end{pmatrix}, \quad (8)$$

$$\zeta_{11} = (\theta_{\mathbf{R}}^2 + \theta_{\mathbf{R}}^3 - \theta_{\mathbf{R}}^1 - \theta_{\mathbf{R}}^4) / 2 = -\zeta_{22},$$

$$\zeta_{12} = (\theta_{\mathbf{R}}^2 + \theta_{\mathbf{R}}^4 - \theta_{\mathbf{R}}^1 - \theta_{\mathbf{R}}^3) / 2 = -\zeta_{21},$$

and

$$C = \begin{pmatrix} 1 & 0 & 0 & 0 \\ 0 & 0 & 0 & 1 \\ 0 & 0 & 1 & 0 \\ 0 & 1 & 0 & 0 \end{pmatrix}, \quad C^2 = I_{4 \times 4}. \quad (9)$$

For a S'-type SP at node- $\mathbf{R}'$ , the transfer matrix is

$$\begin{pmatrix} Z_{4\uparrow}^{\text{in}} \\ Z_{4\downarrow}^{\text{out}} \\ Z_{3\uparrow}^{\text{out}} \\ Z_{3\downarrow}^{\text{in}} \end{pmatrix} = T_{\mathbf{R}'} \begin{pmatrix} Z_{1\uparrow}^{\text{out}} \\ Z_{1\downarrow}^{\text{in}} \\ Z_{2\uparrow}^{\text{in}} \\ Z_{2\downarrow}^{\text{out}} \end{pmatrix}, \quad (10)$$

$$T_{\mathbf{R}'} = \begin{pmatrix} -J_{21}^{-1} J_{22} & J_{21}^{-1} \\ J_{12} - J_{11} J_{21}^{-1} J_{22} & J_{11} J_{21}^{-1} \end{pmatrix}, \quad (11)$$

$$J = C (P_{\mathbf{R}'} \otimes Q_{\mathbf{R}'}^\dagger) C, \quad (12)$$

where

$$P_{\mathbf{R}'} = \begin{pmatrix} \frac{1}{\sqrt{1-p}} e^{i\omega_{11}} & -\sqrt{\frac{p}{1-p}} e^{i\omega_{12}} \\ -\sqrt{\frac{p}{1-p}} e^{i\omega_{21}} & \frac{1}{\sqrt{1-p}} e^{i\omega_{22}} \end{pmatrix} \quad (13)$$

$$\omega_{11} = (\theta_{\mathbf{R}'}^1 + \theta_{\mathbf{R}'}^2 + \theta_{\mathbf{R}'}^3 + \theta_{\mathbf{R}'}^4) / 2 = -\omega_{22},$$

$$\omega_{12} = (\theta_{\mathbf{R}'}^2 + \theta_{\mathbf{R}'}^3 - \theta_{\mathbf{R}'}^1 - \theta_{\mathbf{R}'}^4) / 2 = -\omega_{21},$$

and

$$\begin{aligned} Q_{\mathbf{R}'} &= \begin{pmatrix} \sqrt{1-q}e^{i\chi_{11}} & \sqrt{q}e^{i\chi_{12}} \\ -\sqrt{q}e^{i\chi_{21}} & \sqrt{1-q}e^{i\chi_{22}} \end{pmatrix} \\ \chi_{11} &= (\theta_{\mathbf{R}'}^1 + \theta_{\mathbf{R}'}^2 - \theta_{\mathbf{R}'}^3 - \theta_{\mathbf{R}'}^4)/2 = -\chi_{22}, \\ \chi_{12} &= (\theta_{\mathbf{R}'}^1 + \theta_{\mathbf{R}'}^3 - \theta_{\mathbf{R}'}^2 - \theta_{\mathbf{R}'}^4)/2 = -\chi_{21}. \end{aligned} \quad (14)$$

Then the transfer matrix for the  $k$ -th PL is

$$T^{(k)} = V_4^{(k)} V_3 V_2^{(k)} V_1, \quad (15)$$

here  $V_1$  is the transfer matrix of the sub-layer composed merely by S-type SPs with the following form

$$V_1 = \text{diag}(T_{\mathbf{R}}, \dots, T_{\mathbf{R}})_{W\text{-blocks}}, \quad (16)$$

$V_3$  is the transfer matrix of the S'-type sub-layer

$$V_3 = \begin{pmatrix} B_1 & 0 & \cdots & 0 & B_2 \\ 0 & T_{\mathbf{R}'} & \cdots & 0 & 0 \\ \vdots & \vdots & \ddots & \vdots & \vdots \\ 0 & 0 & \cdots & T_{\mathbf{R}'} & 0 \\ B_3 & 0 & \cdots & 0 & B_4 \end{pmatrix}, \quad (17)$$

where  $B_{1,2,3,4}$  are  $2 \times 2$  matrices and determined by the choice of boundary condition in transverse direction. When we focus on the edge modes, the reflecting boundary condition (RBC) is imposed. The Kramers pair is totally reflected without any spin mixing at boundary nodes, thus

$$\begin{pmatrix} B_4 & B_3 \\ B_2 & B_1 \end{pmatrix} = I_{4 \times 4}. \quad (18)$$

If the bulk behavior is the main concern, the periodic boundary condition (PBC) is adopted, which means

$$\begin{pmatrix} B_4 & B_3 \\ B_2 & B_1 \end{pmatrix} = T_{\mathbf{R}'}. \quad (19)$$

At last,  $V_2^{(k)}$  and  $V_4^{(k)}$  are  $4W \times 4W$  intra- and inter- PL random-phase-factor matrices,

$$[V_{\alpha}^{(k)}]_{lm} = \delta_{lm} e^{i\phi_{\alpha,l}^{(k)}}, \quad (\alpha = 2, 4), \quad (20)$$

where  $\phi_{\alpha,l}^{(k)}$  are independently and uniformly distributed in  $[0, 2\pi)$ . Multiplying  $T^{(k)}$  sequentially, the total transfer matrix  $T_W^L$ , which relates the electron flows on the left of the system  $(Z_{1\uparrow}^L, Z_{1\downarrow}^L, \dots, Z_{2W\uparrow}^L, Z_{2W\downarrow}^L)^T$  and those on the right  $(Z_{1\uparrow}^R, Z_{1\downarrow}^R, \dots, Z_{2W\uparrow}^R, Z_{2W\downarrow}^R)^T$ , is then obtained as

$$\begin{pmatrix} Z_{1\uparrow}^{R,o} \\ Z_{1\downarrow}^{R,i} \\ Z_{1\downarrow}^R \\ \vdots \\ Z_{2W\uparrow}^{R,i} \\ Z_{2W\downarrow}^{R,o} \end{pmatrix} = T_W^L \begin{pmatrix} Z_{1\uparrow}^{L,i} \\ Z_{1\downarrow}^{L,o} \\ Z_{1\downarrow}^L \\ \vdots \\ Z_{2W\uparrow}^{L,o} \\ Z_{2W\downarrow}^{L,i} \end{pmatrix}, \quad T_W^L = T^{(L)} \dots T^{(1)}. \quad (21)$$

By introducing a unitary matrix  $O$ , with

$$O_{st} = \begin{cases} 1, & \begin{aligned} (s,t) &= (4k-3, k) \text{ or} \\ (s,t) &= (4k-2, 3W+k) \text{ or} \\ (s,t) &= (4k-1, 2W+k) \text{ or} \\ &k=1, \dots, W \end{aligned} \\ 0, & \text{otherwise} \end{cases}, \quad (22)$$

the electron flows on each side of the system are reordered into four subgroups marked by  $(\alpha = i/o, \sigma = \uparrow/\downarrow)$ , i.e.,

$$\begin{pmatrix} Z_{o,\uparrow}^R \\ Z_{o,\downarrow}^R \\ Z_{i,\uparrow}^R \\ Z_{i,\downarrow}^R \end{pmatrix} = \tilde{T} \begin{pmatrix} Z_{i,\uparrow}^L \\ Z_{i,\downarrow}^L \\ Z_{o,\uparrow}^L \\ Z_{o,\downarrow}^L \end{pmatrix}, \quad \tilde{T} = O^\dagger T_W^L O. \quad (23)$$

Generally, the charge and spin transport of the sample is described by a  $4W \times 4W$  scattering matrix  $S_t$ ,

$$\begin{pmatrix} Z_{o,\uparrow}^L \\ Z_{o,\downarrow}^L \\ Z_{i,\uparrow}^L \\ Z_{i,\downarrow}^L \end{pmatrix} = S_t \begin{pmatrix} Z_{i,\uparrow}^R \\ Z_{i,\downarrow}^R \\ Z_{o,\uparrow}^R \\ Z_{o,\downarrow}^R \end{pmatrix}, \quad S_t = \begin{pmatrix} R & T' \\ T & R' \end{pmatrix}, \quad (24)$$

where  $T$  and  $T'$  ( $R$  and  $R'$ ) are  $2W \times 2W$  transmission (reflection) matrices. The Landauer formula tells us that the total charge conductance  $G$  is

$$G = \frac{e^2}{h} \text{Tr}(T'^\dagger T'). \quad (25)$$

Finally, by comparing Eqs. (23) and (24),

$$\tilde{T} = \begin{pmatrix} \tilde{T}_{11} & \tilde{T}_{12} \\ \tilde{T}_{21} & \tilde{T}_{22} \end{pmatrix} = \begin{pmatrix} T - R'T'^{-1}R & R'T'^{-1} \\ -T'^{-1}R & T'^{-1} \end{pmatrix}. \quad (26)$$

one finally has  $T' = (\tilde{T}_{22})^{-1}$ .

This provides the main algorithm of calculating the two-terminal conductance. Before ending this subsection, a few points need to be addressed. First,  $\Theta_{\mathbf{R}(\mathbf{R}')}^{jklm}$  may be simplified to unit matrices therefore randomness only manifests itself in Eq. (20). Second, during the calculation of  $\tilde{T}_{22}$ , the numerical instability of multiplying iteratively  $T^{(k)}$ ,  $k = 1, \dots, L$  can be fixed by performing QR decompositions where needed. Third, except for charge transport, we also can study spin transport within this framework.

## II.D Lyapunov exponents and normalized localization length

For a quasi-one-dimensional (Q1D) system ( $W$  finite,  $L \rightarrow \infty$ ), generally the Anderson localization effect makes the two-terminal transmission decays exponentially. The corresponding decay length is called the Q1D

localization length  $\xi_W$ , which is the function of chemical potential ( $p$ ), SMT ( $q$ ) and transverse dimension  $W$ .

Now we define a real  $4W \times 4W$  symmetric matrix

$$\Omega = \ln \left[ (T_W^L)^\dagger T_W^L \right]. \quad (27)$$

The TRS makes the  $4W$  eigenvalues of  $\Omega$  doubly degenerate into  $2W$  pairs, and further fall into  $W$  groups with opposite sign due to the current conservation request. In other words, the eigenvalues of  $\Omega$  can be written as  $\pm\omega_i, i = 1, \dots, 2W$  meantime satisfying  $\omega_1 = \omega_2 < \omega_3 = \omega_4 < \dots < \omega_{2W-1} = \omega_{2W}$ . The Lyapunov exponents (LEs) associated with this Q1D network system with fixed width  $W$  are then defined by the following limit

$$\Gamma_i = \lim_{L \rightarrow \infty} \omega_i / (2L), \quad (28)$$

and are self-averaging random variables.

The Q1D localization length of electrons is defined as the reciprocal of the smallest positive LE,

$$\xi_W = 1/\Gamma_1, \quad (29)$$

since the decay of the transmission should be controlled by the lowest decay rate in this system. Finally, the criticality of the 2D system is determined by the normalized localization length  $\Lambda$ ,

$$\Lambda \equiv \xi_W / W, \quad (30)$$

as the transverse dimension  $W$  approaches to infinity: if  $\Lambda \rightarrow 0$  or finite ( $W \rightarrow \infty$ ), the system falls into OI phase; if  $\Lambda \rightarrow \infty$  ( $W \rightarrow \infty$ ), the system turns to be metallic.

In general, we do not calculate the LEs by directly diagonalizing  $\Omega$ , which comes from iterative multiplication of transfer matrices and turns to be unstable. Following Ref.[40], we employ the following algorithm to achieve satisfactory estimations for both the LEs and their precision. For simplicity, suppose  $L = s \cdot r \cdot m$ , where  $s, r, m$  are integers. To estimate the largest  $n$  LEs (here  $n = 2L$  to obtain  $\Gamma_1$ ), a  $4W \times n$  matrix  $K^{(0)}$  with random orthogonal columns is multiplied to  $T^{(1)}$ . We then perform the following QR decomposition every  $m$  steps,

$$K^{(j)} M^{(j)} = \left[ T^{(jm)} \dots T^{((j-1)m+1)} \right] K^{(j-1)}, \quad (31)$$

where  $j = 1, \dots, sr$ ,  $K^{(j)}$  are  $4W \times n$  matrices with orthogonal columns and  $M^{(j)}$  are  $n \times n$  upper triangular matrices with positive diagonal elements.

The total length  $L$  is divided into  $s$  segments and each consists of  $r \cdot m$  PLs. In each segment, we calculate,

$$\gamma_i^{(k)} = \frac{1}{rm} \sum_{j=(k-1)r+1}^{kr} \left[ \ln M_{i,i}^{(j)} \right], \quad k = 1, \dots, s. \quad (32)$$

The  $n$  largest LEs are then evaluated as,

$$\Gamma_i = \bar{\gamma} = \frac{1}{s} \sum_{k=1}^s \gamma_i^{(k)}. \quad (33)$$

If each segment ( $rm$ ) is large enough, it is reasonable to assume that  $\gamma_i^{(k)}$  are statistically independent. The standard error  $\sigma_i$  of  $\Gamma_i$  is given by,

$$\sigma_i = \frac{1}{\sqrt{s-1}} \left( \overline{\gamma^2} - \bar{\gamma}^2 \right)^{1/2}, \quad \overline{\gamma^2} = \frac{1}{s} \sum_{k=1}^s \left( \gamma_i^{(k)} \right)^2. \quad (34)$$

In most cases,  $\epsilon_1 = \sigma_1/\Gamma_1 = 2\%$  is an acceptable criterion for a good estimation of  $\Gamma_1$  and then  $\Lambda$ .

### III. RESULTS

#### III.A Phase diagram of SD-QNM with RBC

Following the above algorithms, the phase diagram of the SD-QNM is investigated based on the finite-size scaling analyses of two-terminal conductances and the normalized localization length of electrons. The output for RBC is shown in Fig. 3. Different from the existing results[33–38], our results clearly show that although this network model processes Wigner-Dyson symplectic symmetry, there is no intermediate metallic phase when the SMT emerges. In the entire parameter space, which is the unit square ( $0 \leq p, q \leq 1$ ), OI phase dominates. QSH states only survive on the line segment  $\{0 < p < 0.5, q = 0\}$  as we have chosen S'-type SPs as boundary nodes.

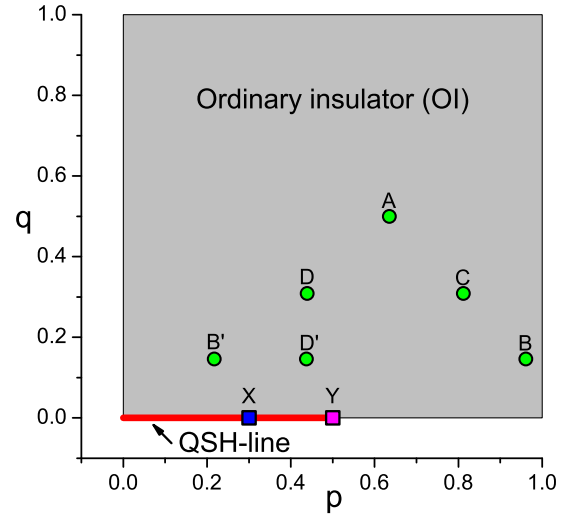


FIG. 3: (Color online) Phase diagram of the SD-QNM for RBC. OI phase (gray area) dominates in the parameter space and QSH phase (red solid line) only survives on the line segment  $\{0 < p < 0.5, q = 0\}$ . The six points  $A, B, B', C, D, D'$  are the same with those in Ref. [36]. The actual coordinates for  $X, Y$  are:  $X : (0.3, 0)$  and  $Y : (0.5, 0)$ .



### III.B QSH-OI transition when $q = 0$

When the SMT is absent ( $q = 0$ ), the SD-QNM is just two copies of CC-RNM with opposite chirality. Consider the case in which RBC is imposed on the network. When  $p \rightarrow 0$ , the quantum tunneling  $t = \sqrt{1-p}$  defeats the percolation amplitude  $r = \sqrt{p}$  along an equipotential line. At S-type SPs (see Fig. 1c), the incoming electron flow with up spin at terminal-1 tends to be scattered to terminal-4 rather than terminal-2. Thus at the upper (lower) edge of the system, a left-to-right (right-to-left) edge mode with up spin emerges. For spin-down electrons, the situation is similar. In summary, a Kramers doublet resides on each edge and this results in the QSH state, as shown in Fig. 4a. On the contrary, when  $p \rightarrow 1$  the quantum tunneling gets weak and the percolation along equipotential lines dominates. In this situation, all electron current loops around potential valleys become close. This results in the OI state (see Fig. 4b). Between these two phases,  $p = 0.5$  (Y point in Fig. 3) is the critical point, which can be obtained from the infinitesimal Migdal-Kadanoff transformation for real-space renormalization of CC-RNM[44].

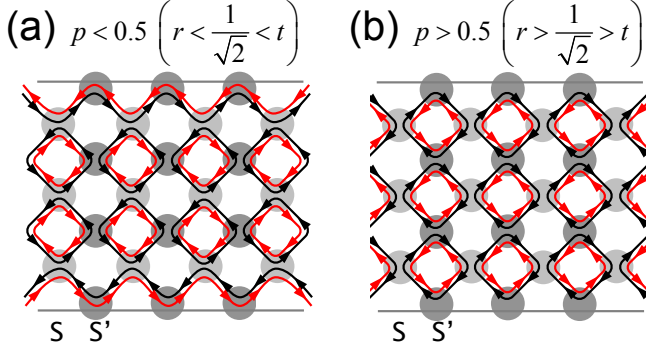


FIG. 4: (Color online) Electron flows distribution of SD-QNM with RBC in different phases in the absence of SMT ( $q = 0$ ). (a) The QSH phase when  $p < 0.5$ . A Kramers doublet resides on each edge of the sample. (b) The OI phase when  $p > 0.5$ . All the electron flows around potential valleys are closed thus makes the system insulating.

The above qualitative picture can be verified by quantitative calculations. The QSH phase for  $p < 0.5$  and OI phase for  $p > 0.5$  can be easily checked by different quantized value (i.e. 2 or 0) of two-terminal conductance. We then perform finite-size scaling calculations of reduced electron localization length for quasi-infinite stripes with different widths to study the criticality at  $p = 0.5$ . The results are shown in Fig. 5. In this calculate, first the PBC is adopted to eliminate the effect of metallic edge states in QSH phase. Second, the relative standard error of the first LE, i.e.  $\epsilon_1$ , is set to be 1%. Third, the sample number is chosen to be 10. The data in Fig. 5 clear show that at  $q = 0.5$ ,  $\Lambda$  increases when the system width gets larger. While for other  $q$ ,  $\Lambda$  decreases as the system gets

wider. This is the clear signal that  $q = 0.5$  is the critical point when  $q = 0$ .

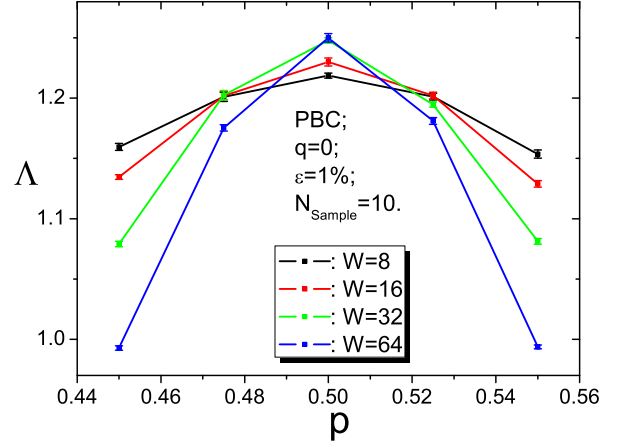


FIG. 5: (Color online) Finite-size scaling results of the reduced electron localization length  $\Lambda$  around  $p = 0.5$  when SMT is absent ( $q = 0$ ). PBC is imposed to eliminate the effect of edge metallic states in QSH phase. The relative standard error of the first LE is set to be 1% and the sample number is 10.

### III.C Direct transition from QSH to OI phases when $q > 0$

Next we turn on the SMT. Our results show that the QSH phase is absolutely unstable to the SMT. This means no matter how small the SMT is, the QSH state will be destroyed completely. To see this, we take the point X ( $p = 0.3, q = 0$ ) in Fig. 3 as an example. To perform a finite-size scaling analysis, we set  $W = L$  and vary  $W$  from  $2^1$  to  $2^9$  within the limitation of our computing power. The average two-terminal conductance  $\langle G \rangle$  and the corresponding error for 128 independent configurations are calculated and plotted in Fig. 6. In these calculations,  $\Theta_{\mathbf{R}(\mathbf{R}')}^{jklm}$  still contain random phases distributing uniformly and independently in  $[0, 2\pi)$ .

For point X, numerical data (solid circles in Fig. 6) show that when the system size increases to  $2^9$ ,  $\langle G \rangle$  approaches the quantized value 2, with the standard error as small as  $5.6 \times 10^{-9}$ . This validates that point X belongs to the QSH phase. Next we perform calculations for  $q = 0.01$ . The result is shown in Fig. 6 by open diamonds. As the system size gets larger,  $\langle G \rangle$  falls to  $10^{-3}$  or even smaller. We then gradually decrease  $q$  by an order of magnitude and calculate the corresponding  $\langle G \rangle$  until  $q$  reaches  $1.0 \times 10^{-6}$ . The results are plotted in Fig. 6 by different symbols connected by lines just for guidance for eyes. The data show that as  $q$  decreases, the deviation of  $\langle G \rangle$  from quantized value 2 gets weaker at  $W = L = 2^9$ . However, it always exists. Even for  $q = 1.0 \times 10^{-6}$  (open circles), if the system size is further increased to  $2^{10}$ ,  $\langle G \rangle$

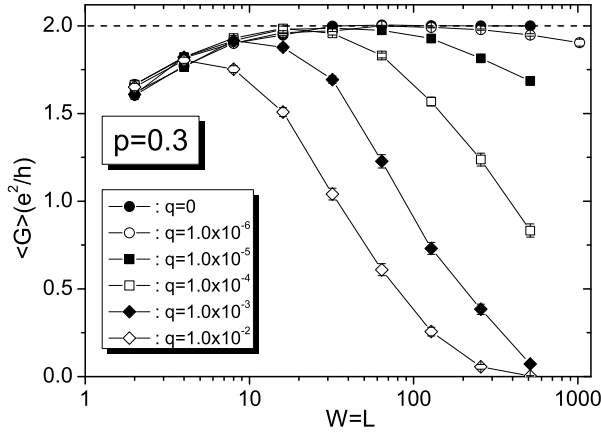


FIG. 6: Evolution of two-terminal conductance  $\langle G \rangle$  at point X ( $p = 0.3, q = 0$ ) when SMT ( $q$ ) appears. The system size increases from  $2^1$  to  $2^9$  for  $q = 0, 10^{-2}, 10^{-3}, 10^{-4}, 10^{-5}$  and  $10^{-6}$  with the sample numbers all equal to 128. In particular, for  $q = 10^{-6}$ , the system size increases further to  $2^{10}$  with the sample number being 16.

deviates from 2 evidently. Limited by the computation power, we can not perform calculations to the system size at which  $\langle G \rangle$  falls to zero. However, the results in Fig. 6 clearly show that the QSH state can not survive when SMT emerges, no matter how small it is.

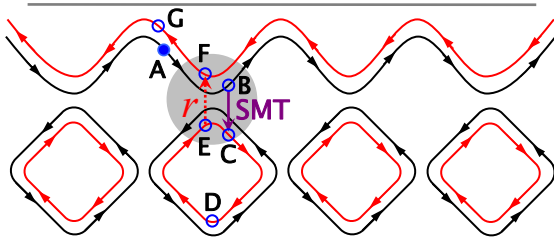


FIG. 7: (Color online) Graphic description of the backscattering process induced by SMT. The light gray circle indicates a S-type SP. With the help of a closed loop around potential peaks, the SMT realizes a “ $A \rightarrow B \rightarrow C \rightarrow D \rightarrow E \rightarrow F \rightarrow G$ ” backscattering thus completely destroys the QSH state.

This result can be understood by the physical process sketched in Fig. 7. Initially the system is in QSH phase, i.e. the situation depicted in Fig. 4a. For simplicity, we take the part around the upper edge as an example and redraw it in Fig. 7 as the basis of our discussion. We focus on an electron with up spin propagating in the dissipationless left-to-right edge channel. Suppose at some moment, the electron is at point A which is set as the starting point. When SMT is absent, the electron at most tunnels into the closed loops with up spins and can not fall into trajectories associated with down spins. Hence the electron will never be backscattered into the right-to-left edge channel with down spin at the upper edge. On the other hand, the backscattering into the right-to-left edge channel with up spin at the lower edge

(not depicted in Fig. 7) by means of multi-tunnelings through closed loops will be suppressed when the system size is large enough since this is a higher-order process. When SMT is turned on, the situation will be completely different. When a spin-up electron propagates from point A and reaches point B, the SMT process at this S-type SP allows it to tunnel into the closed loop associated with down spins (point C on the red loop in Fig. 7). After circling this loop (C to D to E), the electron comes back to this SP and tunnels into the right-to-left edge channel (point F) with down spin via the normal quantum tunneling process and then go to point G and even leftward. Now we realize a backscattering process ( $A \rightarrow B \rightarrow C \rightarrow D \rightarrow E \rightarrow F \rightarrow G$ ) which includes only one step of SMT. Therefore this process is not a higher-order one and should take effect as long as the SMT appears. Combining with the fact that a number of S-type SPs distribute along the upper edge, it is understandable that the QSH state should be absolutely unstable with respect to the SMT.

### III.D The OI phase

We then move to the OI phase. In our phase diagram (see Fig. 3), the six points, A, B, B', C, D, D', are the same as those indicated in the third figure of Ref. [36], except that they are the mirror images of their counterparts in Ref. [36] about the vertical  $p = 0.5$  line since we set S'-type SPs as our boundary nodes while they chose S-type. The finite-size scaling results of  $\langle G \rangle$  for each point with RBC are plotted in Fig. 8 with the sample number always being 128. For points A, B', D and D', the system size increases from  $2^1$  to  $2^9$ . Further increase of system size is out of our existing computing ability. Numerical data show that the average conductances for these four points all tend to decrease when the system size increases. Since we have known that in the metallic phase of systems with symplectic symmetry, the averaged conductance should increase with logarithm of system size due to the anti-localization process[45]. Our data clearly show that the system at these four points falls into neither QSH nor metallic phase. The only possibility is the OI phase. For point B and C, the system size only grows to  $2^8$  which is enough since at this dimension  $\langle G \rangle$  for both cases decreases rapidly to less than  $10^{-10}$ . Thus they should belong to the OI phase. For point B, our data reproduce the result of Ref. [36]. For point C, to further verify our conclusion, the conductance distribution for system size of  $2^7 \times 2^7$  with RBC is calculated and plotted in the inset of Fig. 8d by solid squares. The sample number is  $10^4$ . It turns out that the distribution function of the logarithm conductance  $P[\ln(G)]$  can be well fitted by a Gaussian function, as shown by the solid red curve. This further confirms our conclusion that point C undoubtedly belongs to the OI phase.

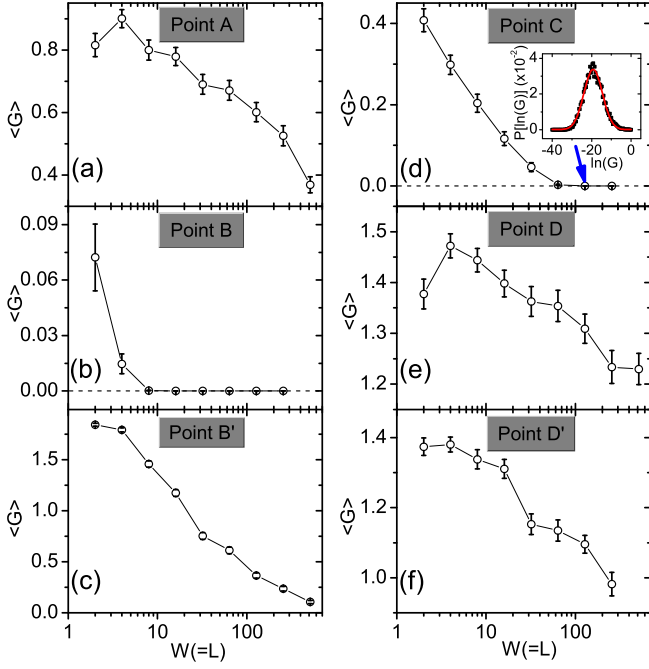


FIG. 8: (Color online) Finite-size scaling results of the two-terminal conductance with RBC for the six points in Ref. [36]. In most cases, the system size increases from  $2^1$  to  $2^9$ . The error bars come from the average process from 128 independent samples for each case. Inset of (d): the black solid squares are the calculated conductance distribution  $P[\ln(G)]$  with RBC for  $W = L = 128$  and  $10^4$  samples. They can be well fitted by a Gaussian function (red curve).

Next, the finite-size scaling calculates of the normalized electron localization length  $\Lambda$  for  $q = 0.3$  and  $q = 0.6$  are performed and the data are plotted in Fig. 9. In these calculates, RBC in transverse direction is adopted and the sample number is chosen to be 100. In addition, the relative standard error of the first LE is set to be 2%. The numerics clearly shows that for both SMT strengths,  $\Lambda$  shrinks when the system size increases. This is the significant signal that along  $q = 0.3$  and  $q = 0.6$  lines, the system falls into OI phase. Similar calculations have been performed for other nonzero  $q$ -values. All results support our conclusion that there are no intermediate metallic phase and the OI phase fills the entire unit square in  $(p, q)$ -parameter space.

#### IV. CONCLUSIONS

In this work, we have reinvestigated in detail the phase transitions in symplectic disordered QSH systems described by a SD-QNM generalized from the famous CC-RNM. The uniqueness of this model lies in the introduction of the SMT at the potential SPs. It induces backscatterings between the Krammers doublet at the same edge and hence completely destroys them, leading

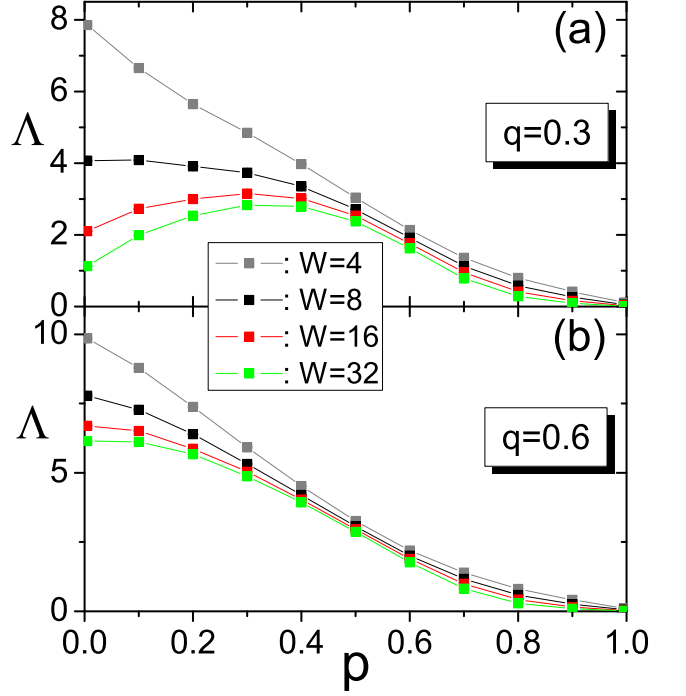


FIG. 9: (Color online) Finite-size scaling results of the reduced electron localization length  $\Lambda$  along (a)  $q = 0.3$  and (b)  $q = 0.6$  with RBC in transverse direction. The relative standard error of the first LE is set to be 2% and the sample number is 100.

to a direct transition between the QSH and OI phases. We have performed finite-size scaling analyses of two-terminal conductance and normalized localization length of electrons. All numerical data strongly support this picture. Our results answers partially the question raised in the beginning of this paper: for disordered QSH systems belonging to the Wigner-Dyson symplectic class AII, at least in the framework of the SD-QNM with SMT at potential SPs, a direct transition between the QSH and OI phases exists.

#### ACKNOWLEDGEMENT

We thank Prof. X. R. Wang and Prof. G. Xiong for fruitful discussions. This work is supported by the Science Foundation for The Excellent Youth Scholars of Educational Commission of Hebei Province, China (Grant No. Y2012027) and the Natural Science Foundation of Hebei Province, China (Grant No. A2014205080). J.L also acknowledges the support from the National Natural Science Foundation of China (Grant Nos. 11374088 and 11104060).



---

\* Electronic address: jlu@hebtu.edu.cn

- [1] P. W. Anderson, Phys. Rev. **109**, 1492 (1958).
- [2] P. A. Lee and T. V. Ramakrishnan, Rev. Mod. Phys. **57**, 287 (1985).
- [3] B. Kramer and A. MacKinnon, Rep. Prog. Phys. **56**, 1469 (1993).
- [4] B. Huckestein, Rev. Mod. Phys. **67**, 357 (1995).
- [5] F. Evers and A. D. Mirlin, Rev. Mod. Phys. **80**, 1355 (2008).
- [6] M. R. Zirnbauer, J. Math. Phys. **37**, 4986 (1996).
- [7] A. Altland and M. R. Zirnbauer, **55**, 1142 (1997).
- [8] M. Caselle and U. Magnea, Phys. Rep. **394**, 41 (2004).
- [9] P. Heinzner, A. Huckleberry, and M. R. Zirnbauer, Commun. Math. Phys. **257**, 725 (2005).
- [10] E. P. Wigner, Ann. Math. **53**, 36 (1951).
- [11] F. J. Dyson, J. Math. Phys. **3**, 1199 (1962).
- [12] M. Janssen, Int. J. Mod. Phys. B **8**, 943 (1994).
- [13] C. Mudry, C. Chamon, and X.-G. Wen, Nucl. Phys. B **466**, 383 (1996).
- [14] F. Evers and A. D. Mirlin, Phys. Rev. Lett. **84**, 3690 (2000).
- [15] F. Evers, A. Mildenberger, and A. D. Mirlin, Phys. Rev. B **64**, 241303R (2001).
- [16] H. Obuse and K. Yakubo, Phys. Rev. B **69**, 125301 (2004).
- [17] H. Obuse, A. R. Subramaniam, A. Furusaki, I. A. Gruzberg, and A. W. W. Ludwig, Phys. Rev. Lett. **98**, 156802 (2007).
- [18] H. Obuse, A. R. Subramaniam, A. Furusaki, I. A. Gruzberg, and A. W. W. Ludwig, Phys. Rev. B **82**, 035309 (2010).
- [19] A. D. Mirlin, Phys. Rep. **326**, 259 (2000).
- [20] G. Xiong, S.-D. Wang, Q. Niu, D.-C. Tian, and X. R. Wang, Phys. Rev. Lett. **87**, 216802 (2001).
- [21] G. Xiong, S.-D. Wang, Q. Niu, Y. P. Wang, X. C. Xie, D.-C. Tian, and X. R. Wang, J. Phys.: Condens. Matter **18** 2029 (2006).
- [22] H. Obuse and K. Yakubo, Phys. Rev. B **71**, 035102 (2005).
- [23] A. M. Garcia-Garcia and E. Cuevas, Phys. Rev. B **75**, 174203 (2007).
- [24] M. Z. Hasan and C. L. Kane, Rev. Mod. Phys. **82**, 3045 (2010).
- [25] X.-L. Qi and S.-C. Zhang, Rev. Mod. Phys. **83**, 1057 (2011).
- [26] C. W. J. Beenakker, Rev. Mod. Phys. **87**, 1037 (2015).
- [27] Y. F. Ren, Z. H. Qiao, and Q. Niu, Rep. Prog. Phys. **79**, 066501 (2016).
- [28] A. Bansil, H. Lin, and T. Das, Rev. Mod. Phys. **88**, 021004 (2016).
- [29] E. Witten, Rev. Mod. Phys. **88**, 035001 (2016).
- [30] C.-K. Chiu, J. C. Y. Teo, A. P. Schnyder, and S. Ryu, Rev. Mod. Phys. **88**, 035005 (2016).
- [31] I. C. Fulga, F. Hassler, and A. R. Akhmerov, Phys. Rev. B **85**, 165409 (2012).
- [32] S. Ryu, C. Mudry, H. Obuse, and A. Furusaki, Phys. Rev. Lett. **99**, 116601 (2007).
- [33] S. Ryu, C. Mudry, H. Obuse, and A. Furusaki, New J. Phys. **12**, 065005 (2010).
- [34] H. Obuse, A. Furusaki, S. Ryu, and C. Mudry, Phys. Rev. B **76**, 075301 (2007).
- [35] H. Obuse, A. Furusaki, S. Ryu, and C. Mudry, Phys. Rev. B **78**, 115301 (2008).
- [36] K. Kobayashi, T. Ohtsuki, H. Obuse, and K. Slevin, Phys. Rev. B **82**, 165301 (2010).
- [37] H. Obuse, S. Ryu, A. Furusaki, and C. Mudry, Phys. Rev. B **89**, 155315 (2014).
- [38] K. Kobayashi, T. Ohtsuki, and K. Slevin, Int. J. Mod. Phys. Conf. Ser. **11**, 114 (2012).
- [39] S. Ryu and K. Nomura, Phys. Rev. B **85**, 155138 (2012).
- [40] K. Slevin and T. Ohtsuki, New J. Phys. **16**, 015012 (2014).
- [41] C. Wang, Y. Su, Y. Avishai, Y. Meir, and X. R. Wang, Phys. Rev. Lett. **114**, 096803 (2015).
- [42] J. T. Chalker and P. D. Coddington, J. Phys. C **21**, 2665 (1988).
- [43] B. Kramer, T. Ohtsuki, and S. Kettmann, Physics Reports **417**, 211 (2005).
- [44] D. P. Arovas, M. Janssen, and B. Shapiro, Phys. Rev. B **56**, 155138 (1997).
- [45] S. Hikami, A. I. Larkin, and Y. Nagaoka, Prog. Theor. Phys. **63**, 707 (1980).